Desalination and Water Treatment
www.deswater.com
doi: 10.1080/19443994.2013.859101

53 (2015) 1986–1994
February

Taylor & Francis
Taylor & Francis Group

Comprehensive evaluation of adsorption and degradation of tetracycline and oxytetracycline by nanoscale zero-valent iron

Özge Hanay*, Hande Türk

Faculty of Engineering, Department of Environmental Engineering, Firat University, Elazig 23119, Turkey
Tel. +90 424 2370000-5623; Fax: +90 424 2415526; email: ohanay@firat.edu.tr

Received 21 August 2013; Accepted 11 October 2013

ABSTRACT

The interaction of tetracycline (TC) and oxytetracycline (OTC) with nanoscale zero-valent iron (nZVI) was examined with a batch experimental series in order to determine the removal efficiency and transformation products. Experimental variables, such as solution pH, nZVI dosage, contact time, initial TCs concentration, and reaction temperature, were systematically studied. Adsorption kinetics showed that equilibrium was reached within 2 h according to the pseudo-second-order model. The adsorption behavior was pH-dependent and favored at pH 6 regardless of TC type considered due to electrostatic attraction between nZVI and TCs. The adsorption capacity of TC was more than that of OTC. The results of LC-MS-MS showed that main transformation product was 4-epi-tetracycline for TC and insignificant for OTC. On the other hand, desorption studies exhibited that nZVI adsorbed not only parent compounds but also transformation products. The results showed that the removal mechanism of TC and OTC by using nZVI surface was mainly the adsorption relatively than the degradation process.

Keywords: Nanoscale zero-valent iron; Tetracycline; Oxytetracycline; Transformation product

1. Introduction

Among the most widely studied nanomaterials for water treatment and soil/groundwater remediation processes, metallic iron is environmentally friendly and cheap cost due to a strong reducing agent. Several studies demonstrated that zero valent iron (ZVI) could transform the hazardous organic compounds to less harmful or harmless chemical compounds. Therefore, by using ZVI, there have been several attempts to eliminate various pollutants, including chlorinated organic compounds, nitro-aromatic compounds, pesticides, dyes, and heavy metals [1–5]. Recently, it has been indicated that nano-scale ZVI particles have larger surface area and higher reactivity than micro-scale ones, which provide a higher organic reduction. For example, Fang et al. [6] reported that the removal of antibiotic metronidazole by nZVI was about 49 times higher when compared with commercial iron powder under same dosages. Therefore, the usage of nanoscale ZVI provides several advantages: a decrease in reductant dosage, short reaction time, and control over the risk of release of toxic intermediates.

Tetracyclines (TC) like TC and oxytetracycline (OTC) are a group of broad-spectrum antibiotics used in commonly human, veterinary medicine, and aquaculture for about 70 years [7]. Some researchers have reported the toxic effects of TCs to plants, sewage

*Corresponding author.

sludge bacteria, and non-target organisms such as *Daphnia magna* in aqueous environment [8–10]. Moreover, due to resistance of these compounds against conventional treatment processes, alternative methods such as ultraviolet radiation, ozonation, photocatalysis, photolysis, electrochemical treatment alone or prior to a biological treatment for complete removal have been intensively studied by various researchers [11–14]. On the other hand, a number of materials, such as powdered active carbon, magnetite nanoparticles, single- and multi-walled carbon nanotubes, graphene oxide, goethite, and palygorskite, have been examined in removal of TCs [15–20]. To the best our knowledge, only one study was performed to investigate the effect of reaction conditions on removal of TC by nZVI [7]. This study evaluates the interaction of TC and OTC with nZVI and the transformation products at optimum conditions.

2. Materials and methods

2.1. Chemicals

Hydrochloride salts of TC (CAS No. 64-755) and OTC (CAS No. 2058-46-0) were purchased from Applichem and Sigma, and the chemical structure of TC and OTC is shown in Fig. 1. Ferric chloride (CAS No. 10025-77-1) and sodium borohydride (CAS No. 16940-66-2) were purchased from Sigma. 4-epi-TC (CAS No. 30026) and 4-epi-OTC (CAS No. 30026), anhydrotetracycline (ATC) (CAS No. 30026), α-Apo-oxytetracycline (α-Apo-OTC) (CAS No. 30026) and β-Apo-oxytetracycline (β-Apo-OTC) (CAS No. 30026) were supplied from European Pharmacopoeia Reference Standard, and 4-epi-anhydrotetracycline (CAS No. 13174500) was supplied from Dr. Ehrenstorfer GmbH. Methanol (CAS No. 67-56-1), acetonitrile (CAS No. 75-05-8), and formic acid (CAS No. 23-26-45) from Merck were LC-MS and HPLC grade. Other reagents were also in analytical grade. Reagent water was produced from a Millipore Milli-Q Ultrapure Gradient 3 V purification system. All solutions were prepared with deionized deoxygenated water and stored at 4 ˚C.

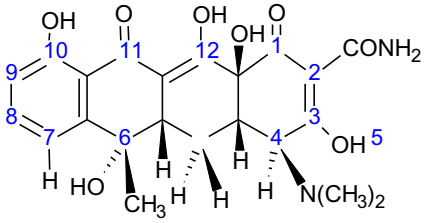

Tetracycline (TC)

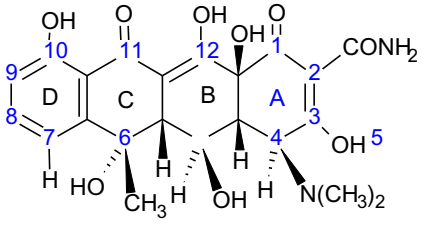

Oxytetracycline (OTC)

Fig. 1. Chemical structures of TC and OTC.

2.2. Synthesis of nZVI

The synthesis of nZVI used in the experiments was performed according to Hwang et al. [21]. They demonstrated that the particle size was decreased about 10 times lower under short reaction time and high reductant concentration. nZVI was synthesized in a 500 mL flask reactor with four open necks. One of the necks housed a tunable mechanical stirrer and the solution was stirred vigorously at 250 rpm. For the reduction in ferric ions to nZVI, a peristaltic pump was used to add 250 mL of borohydride solution into 250 mL of ferric ions solution. Other two necks were used for the inlet and outlet of nitrogen gas to prevent any possible oxidation of iron. nZVI synthesis conditions were as follows: reductant delivery rate: 20 mL min^{-1}, [Fe^{3+}]: 71.7 mM and [BH_4^-]: 358.5 mM. The reduction reaction can be described as follows:

$$4Fe^{3+} + 3BH_4^- + 9H_2O \rightarrow 4Fe^0 + 3H_2BO_3^- + 12H^+ + 6H_2 \quad (1)$$

The resulting gray-black nZVI was collected by vacuum filtration of the solution. The collected particles were then washed 3 times with ethanol, dried, and stored in an anaerobic chamber. The particle size and morphology were determined using scanning electron microscopy (Jeol-JSM-7001F). The specific surface was analyzed with a Brunauer–Emmett–Teller (BET) surface area analyzer. Zeta potential as a function of the solution pH was to determine the isoelectric point of nZVI.

2.3. Batch experiments

Reactions of TCs with nZVI were conducted using 120 mL glass bottles fitted with Teflon-lined septa under a constant stirring. In order to avoid possible photodegradation of TCs, the bottles were wrapped in

aluminum foil. Different factors were investigated,that is, initial solution pH, initial TCs concentration, nZVI dosage, and reaction temperature. In order to determine the effect of initial solution pH on TCs adsorption, pH was varied in the range of 2–9 at initial TCs concentration of 60 mg L^{-1}. The initial pHs were adjusted by adding diluted HCl or NaOH using a digital pH-meter (Orion 3 STAR). The effect of nZVI dosage was investigated at constant TCs concentrations of 60 mg L^{-1} by changing the amount of ZVI from 0.05 to 0.6 g L^{-1}. After adding a desired amount of nZVI particles into the solution, it was ultrasonically dispersed in an ultrasonic cleaning bath (Jeiotech) for 1 min. The effect of temperature on sorption was performed at 60 mg L^{-1} TCs concentration and optimum pH, the temperature was maintained at 30, 45, and 60˚C. Samples aliquots were taken periodically by a syringe and then filtered immediately through 0.22 μm membrane filter prior to TCs analysis by HPLC (Shimadzu). In addition, a control test was carried out according to the same procedure without nZVI. The control experiments showed minimal degradation (<6%) of both TCs during the reaction time studied because of the fact that TCs are known to be degraded as abiotic depending on pH, redox, and light conditions and degradation products can be formed via epimerization, dehydration, and proton transfer pathways [10]. Fate analyses of TC indicate that abiotic degradation products, and reversible epimers, may be formed due to hydrolysis and/or photolysis such as epi-tetracyclines (ETC), and ATC [22]. Moreover, to desorb TCs from the nZVI surfaces, 10 μL of concentrated HCI was added to 1 mL of sample aliquot. The acidified sample was shaken for three minutes and centrifuged for 20 min and then the supernatant was analyzed by HPLC. The concentrations of total dissolved Fe were measured by the atomic absorption spectrophotometer (PerkinElmer 800). All experiments were conducted in duplicate and average results were reported.

2.4. Analysis of TCs

TCs were analyzed by HPLC (Shimadzu) with an AllureBiPh column (5 μm, 150 × 4.6 mm). The mobile phase was composed of a mixture of ammonium dihydrogenphosphate/acetonitrile (20/80, v/v). The flow rate and sample size were 1.2 mL min^{-1} and 100 μL, respectively. TCs were detected at 269 nm by a diode-array detector. The retention time of TC and OTC was found to be 4 and 3.1 min, respectively. Calibration was made with 5 standards between 20 and 100 mg L^{-1}, and R^2 was higher than 0.998.

2.5. LC/MS-MS analysis

Identification of TC and OTC products was achieved by LC-MS-MS (Shimadzu LC-20 AD) with Venusil XBP C18 column (3 μm, 100 Å, 2,1 × 50 mm). The injection volume was 100 μL. Ultrapure water (A) and methanol containing 0.1% formic acid (v/v) (B) were used as mobile phases. Gradient elution was as follows: The initial 5% B was increased to 15% within 6 min; a further 25% B was increased 40% in 6 min. Finally, the gradient was returned to the initial conditions of 5% B for 13 min. The flow rate was 0.3 mL min^{-1} at the column temperature of 40˚C.

2.6. Adsorption kinetics and isotherms

Since adsorption kinetics exhibit the adsorption rate with the contact time of adsorption reaction, the information on adsorption kinetics is also crucial to provide understanding on adsorption mechanism. Based on the equilibrium data, it was observed that the adsorption of TC and OTC increased rapidly at the first two hours before it slowed down and approached equilibrium for more time relatively than 2 h. Therefore, it was evaluated the known adsorption kinetics; the pseudo-first-order and the second-order.

The adsorbed quantity of TCs by nZVI was calculated as Eq. (2);

$$q_e = (C_o - C_e)/m \tag{2}$$

C_o and C_e represent the initial and equilibrium concentrations of TC and OTC (mg L^{-1}), and m is the mass of nZVI used.

The pseudo-first-order reaction rate model known as the Lagergren kinetic equation is widely employed;

$$\frac{dq}{dt} = k_1(q_{eq} - q) \tag{3}$$

where q_{eq} and q are adsorbed TCs quantity per gram of ZVI at equilibrium and any time (mg g^{-1}), respectively, k_1 is the rate constant of pseudo-first-order sorption (min^{-1}). The integrated form of the differential equation becomes,

$$\log(q_{eq} - q) = \log(q_{eq}) - \frac{k_1}{2.303}\, t \tag{4}$$

A plot of log (q_{eq}–q) against t should give a linear relationship with the slope of $k_1/2.303$ and intercept of ($\log q_{eq}$).

The pseudo-second-order kinetic model is also based on the adsorption capacity of the solid phase, and the assumption that the adsorption process involves chemisorption mechanism and is expressed as;

$$\frac{dq}{dt} = k_2(q_{eq} - q)^2 \quad (5)$$

where k_2 is the rate constant of pseudo-second-order adsorption. The integrated form of the differential equation becomes,

$$\frac{t}{q} = \frac{1}{k_2 q_{eq}^2} + \frac{1}{q_{eq}} t \quad (6)$$

In the case of second-order kinetic equation, the plot of t/q against t of Eq. (6) should give a linear relationship that the q_{eq} and k_2 could be determined.

Adsorption isotherms describe how solutes interact with sorbents. Equilibrium sorption isotherms are often described by the Langmuir and Freundlich model.

In Langmuir model:

$$\frac{C_e}{q_m} = \frac{C_e}{q_m} + \frac{1}{K_b q_m} \quad (7)$$

where q_m is the maximum monolayer adsorption (mg g^{-1}), C_e is the equilibrium concentration of TCs (mg L^{-1}), q_e is the amount of TCs adsorbed per unit weight of nZVI at equilibrium concentration (mg g^{-1}), and K_b is the Langmuir constant related to the affinity of binding sites (L mg^{-1}). Langmuir model suggests that the adsorption occurs through monolayer adsorption on homogeneous surface without transformation and interaction between sorbed molecules.

The Freundlich model is an empirical equation based on sorption on a heterogeneous surface, which suggests that binding sites are not equivalent and/or independent. Freundlich equation is expressed as:

$$q_{eq} + K_{F\,C_{eq}} 1/n \quad (8)$$

where K_F is an indicator of the adsorption capacity and n is an indicator of the adsorption intensity.

The Langmuir and Freundlich isotherm constants were determined from the plots of C_e/q_e against C_e, ln q_e vs. ln C_e, respectively, at 30, 45, and 60°C.

3. Results and discussion

3.1. nZVI characterization

It was determined that the particle size of the synthesized nZVI varied in the range of about 35–65 nm by using SEM images (Fig. 2), and its specific surface area became 25 m^2 g^{-1} by BET surface area analysis. The similar particle sizes were also observed by other researchers. For example, Lien and Zhang [23] and Shih et al. [24] found the size distribution in the range of 10–100—50–100 nm, respectively, for nZVI synthesized with the same procedure as liquid-phase reduction method. Our results indicated that nZVI particles had a uniform and spherical shape. The chain-like structures of aggregation may be performed from the magnetic interactions of van der Waals forces between the iron particles [5]. According to EDX analysis, nZVI included 92% iron and 8% oxygen due to the oxidation of the synthesized nanoscale Fe specimen during sample preparation and SEM analysis. This result is similar to the findings of Shih et al. [25].

3.2. Adsorption of TC and OTC with nZVI

3.2.1. Initial concentration and contact time

A series of experiments with varying initial TC and OTC concentrations at constant nZVI dosage were conducted at pH 6 to assess the effect of each reactant on the reaction kinetics. When initial TC and OTC concentrations were increased from 20 to 100 mg L^{-1}, which means an increase in TCs loading rate, TC and OTC removal efficiencies decreased due to limited available surface sites under the constant nZVI dosage. In addition, the effect of contact time on the

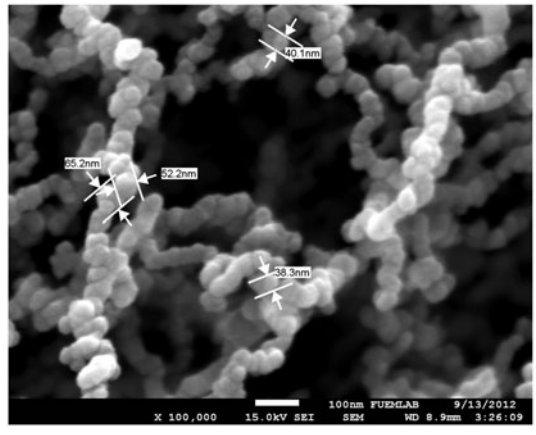

Fig. 2. SEM images of nZVI.

adsorbed amount was performed within 4 h while the amount of nZVI, pH, and initial TCs concentrations was kept constant. As illustrated in Fig. 3, adsorption was higher in TC relatively than OTC, and there was no tangible change in the adsorbed amount (q_e) after 2 h. Therefore, the running time was chosen as 2 h for the following experiments. The maximum adsorbed quantity was found to be 148 and 113 mg g^{-1} for TC and OTC, respectively. These results seem to be in agreement with the literature since it has been reported that adsorption capacity of TC was more than that of OTC [20,26].

3.2.2. Effect of pH

Solution pH is considered as one of the most important factors that affect the removal of contaminants using Fe^0 from water medium [6]. Fig. 4 illustrates that an increase in pH values in the range of pH 2–6 caused an increase in the adsorption efficiencies of both TCs, where nZVI dosage is 0.4 g L^{-1} and an initial concentration of 60 mg L^{-1} TCs at 30°C. The pH of all solutions determined at the end of the reactions is given in Table 1. Increasing initial pH from 4 to 7 affected the removals of TC and OTC by using nZVI. For example, the removal percentages of TC and OTC were 95 and 96% at pH: 4 while those were 99 and 98% at pH: 6, respectively. The highest removal was observed at pHs 5 and 6. TC have several polar/ionizable groups including amino, carboxyl, phenol, alcohol, and ketone, and they exhibit three macroscopic acidity constants. The pKa values were 3.3, 7.7, and 9.7 for TC molecule and 3.3, 7.3, and 9.1 for OTC molecule. As a result, TCs exist as cationic, zwitterionic, and anionic species under acidic, moderately acidic to neutral and alkaline conditions, respectively. Moreover, nZVI was positively charged at pH < 5.38 and negatively charged at pH > 5.38 because the pHzpc of ZVI was found to be 5.38. Electrostatic repulsion between TCs and nZVI surface was negligible at pH near to pH = (pKa_1 + pKa_2)/2, thus creating a maximum electrostatic attraction at the intermediate pH range. On the other hand, considering the pH variations for TC and OTC compounds was important since changes in pH values took placed markedly at the end of reactions (Table 1). At initial pHs > 7, the final pH did not exhibit a significant change. Some researchers also reported that the redox of ZVI particles characteristically increased solution pH [7,23]. According to Eq. (9), in the absence of O_2, Fe^0 oxidized to Fe^{2+} while H^+ is reduced to H_2 and the reduction of H_20 generates OH^- according to Eq. (10) contributing to a significant increase in pH.

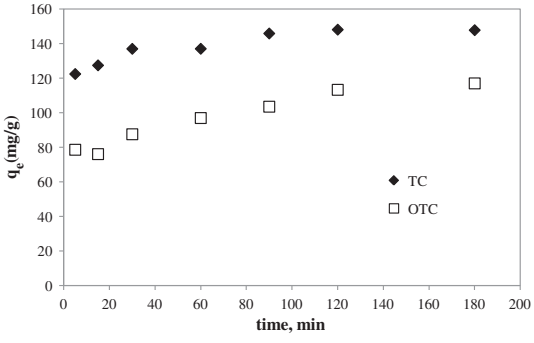

Fig. 3. The effect of contact time on the adsorption of TC and OTC ($Co_{(TC,\ OTC)}$: 60 mg L^{-1}, nZVI: 0.4 g L^{-1}, T: 30°C, pH 6).

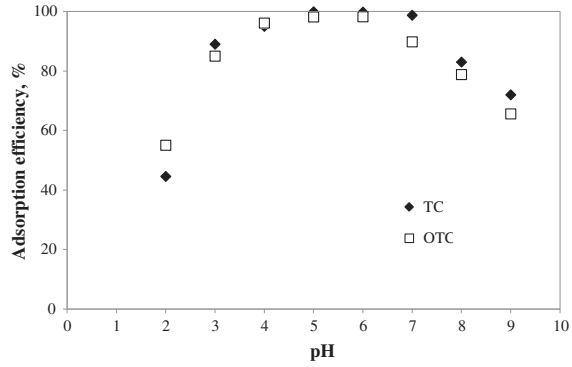

Fig. 4. Effect of pH on TC and OTC adsorption ($Co_{(TC,OTC)}$: 60 mg L^{-1}, T: 30°C, contact time: 2 h, nZVI: 0.4 g L^{-1}).

Table 1
pH variations at the end of reactions

	Final pH	
Initial pH	TC	OTC
2	2.34	2.05
3	5.48	5.29
4	6.65	5.89
5	7.03	6.51
6	7.43	7.09
7	7.70	7.55
8	8.06	8.38
9	9.33	9.75

$$Fe^0 + 2H^- \rightarrow Fe^{2+} + H_2 \quad (9)$$

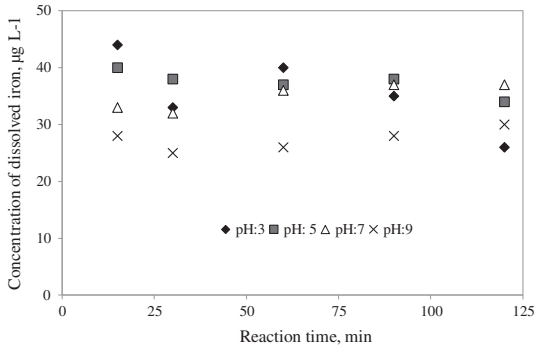

Fig. 5. Total concentration of dissolved iron during the reaction time at different pHs (nZVI: 0.4 g L^{-1}).

$$Fe^0 + 2H_2O \rightarrow Fe^{2+} + H_2 + 2OH^- \quad (10)$$

On the other hand, dissolution of nZVI under the selected experimental conditions (pH: 3, 5, 7, and 9, TCs: 60 mg L^{-1}, nZVI: 0.4 g L^{-1}) was measured during the reaction. As can be seen in Fig. 5, there was no significant amount of dissolved iron within the all pH values.

3.2.3. Effect of nZVI dosage

The influence of nZVI dosage on removal of TCs was studied using 0.05, 0.1, 0.2, 0.4, and 0.6 g L^{-1} of nZVI within 2 h at conditions of initial pH: 6 and TCs concentration: 60 mg L^{-1}. It can be clearly seen from Fig. 6(a) and (b) that higher removal efficiencies for both TCs were obtained at higher ZVI dosages during same running time. The removals of TC and OTC were approximately 71 and 36% at low dosage of 0.05 g L^{-1}, and 97 and 80% at dosage of 0.4 g L^{-1}, respectively. Furthermore, higher removal percentages of OTC within 2 h were not achieved even if iron dosage increased from 0.05 to 0.4 g L^{-1} when compared to TC removal percentages. With an increase to 0.6 g L^{-1} in the nZVI dosage, it was achieved the best result in OTC removal. However, it was not necessary to use a much higher iron dosage since the difference in the removal efficiencies of TC and OTC was rather small. As a result, nZVI dosage of 0.4 and 0.6 g L^{-1} was optimum for the effective removal of TC and OTC within 2 h, respectively.

3.2.4. Kinetics results

The values of k_1, k_2, q_{eq}, and correlation coefficient are compared in Table 2. The calculated q_{eq} values

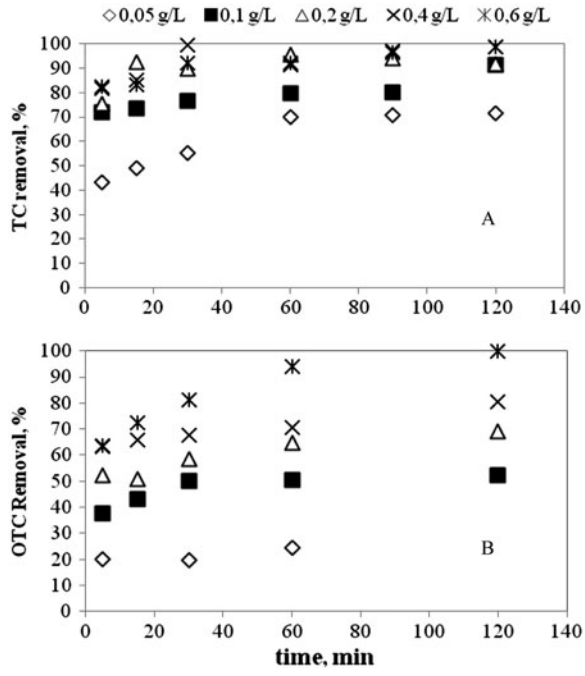

Fig. 6. Effect of nZVI dosage on removal of TC (a) and OTC (b) ($Co_{(TC,\ OTC)}$: 60 mg L^{-1}, T: 30 °C, pH 6).

agreed very well with the experimental q_{eq} values in the case of pseudo-second-order kinetics, while pseudo-first-order model did not give reasonable values. As similar to our present study, the pseudo-second-order kinetics model has been widely applied to the adsorption of TCs by other adsorbents from aqueous solutions in recent years [17,18,20]. The adsorption rate-limiting step may be chemisorptions, and the adsorption of TCs occurs probably via surface complexation reactions at specific sorption sites. The calculated adsorption capacity (q_e) estimated by the pseudo-second-order model was found to be about 145, 147, and 151 mg g^{-1} for TC at temperature of 30, 45, and 60 °C while the detected limited values in experiments were about 142, 142, and 150 mg g^{-1}, respectively. The rate constant of sorption (k) was 0.005, 0.003, and 0.015 g mg^{-1} min^{-1} for TC which were much higher than those of TC, adsorption on graphene oxide (0.065 g mg^{-1} h^{-1}) [20].

Table 3 shows the isothermal constants and the correlation coefficients. It was found that the adsorption of TC and OTC on nZVI correlated well with the Langmuir equation as compared to the Freundlich equation under the studied concentration ranges. However, the maximum adsorption capacity, q_m, for TC is higher than that for OTC. As similar, Zhang et al. (2011) reported that the sorption of TC on multi-walled carbon nanotubes was also described as

Table 2
Change of the pseudo-first- and second-order reaction rate constants with temperature

TCs	T (℃)	q_{eqexp} (mg g^{-1})	First-order kinetic model			Second-order kinetic model		
			k_1 (min^{-1})	$q_{eq,cal}$ (mg g^{-1})	R^2	k_2 (g mg^{-1} min^{-1})	$q_{eq,cal}$ (mg g^{-1})	R^2
TC	30	142.24	0.139	4.90	0.217	0.005	144.93	0.999
	45	142.20	0.029	3.54	0.810	0.003	147.06	0.999
	60	149.98	0.051	2.09	0.735	0.015	151.52	1
OTC	30	98.43	0.058	5.60	0.480	0.001	105.26	0.997
	45	99.51	0.029	3.35	0.789	0.004	102.04	0.999
	60	100.00	0.020	1.26	0.245	0.045	100.00	1

Table 3
Isotherms constants for TC and OTC adsorbed on nZVI

		Langmuir model			Freundlich model		
	T (℃)	q_{max} (mg g^{-1})	K_b (L mg^{-1})	R^2	K_f (mg g^{-1})	n	R^2
TC	30	158.73	157.50	0.955	119.68	6.96	0.260
	45	208.33	60.00	0.976	154.32	5.06	0.638
	60	232.55	6.14	0.879	177.48	4.42	0.700
OTC	30	109.89	5.06	0.943	76.28	3.76	0.678
	45	144.93	2.76	0.989	87.53	4.72	0.700
	60	149.25	6.70	0.997	46.53	4.07	0.610

Langmuir isotherms [27]. The maximum adsorption capacity of TC on nZVI was 158, 208, and 232 mg g^{-1} at 30, 45, and 60℃, respectively, which were higher than q_m achieved on metal oxides such as rectorite (140 mg g^{-1}) and marine sediments (16.7–33.3 mg g^{-1}) while lower than multi-walled carbon nanotubes (269.54 mg g^{-1}) and graphene oxide (313.48 mg g^{-1}) [19,20,28,29].

3.2.5. Transformation products

The transformation products of both TCs were determined at optimum removal conditions in order to evaluate ones, which are dominant for degradation of TCs. The following compounds were determined as follows: ETC, 4-epi-anhydrotetracycline (EATC), ATC, 4-epi-oxytetracycline (EOTC), α-Apo-OTC, and β-Apo-OTC during the reaction time under different initial TCs concentrations.

Transformation products can be formed via the epimerization, dehydration, and proton transfer pathways. It has been reported that TC and OTC can be reversibly epimerized at position C-4 to form the corresponding 4-epimers (ETC, EOTC) in pH values between 2 and 6. As expected, ETC was the dominant transformation product of TC (Fig. 7). The generation

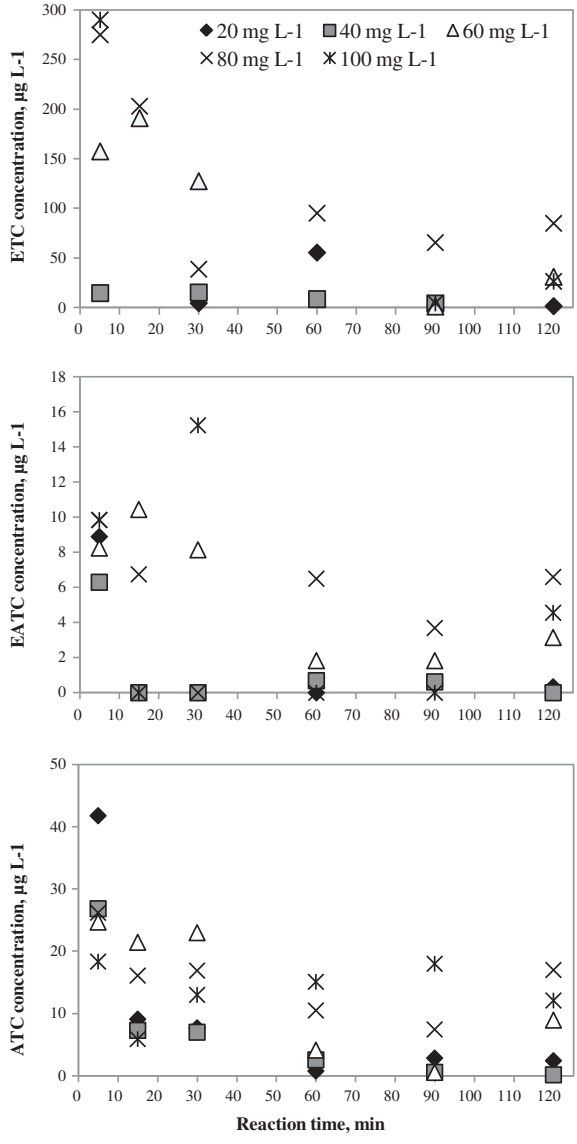

Fig. 7. The concentrations of TC transformation products during the reaction time at different initial TC concentrations ($Co_{(TC,)}$: 20–100 mg L^{-1}, T: 30℃, pH 6, nZVI: 0.4 g L^{-1}).

of ETC was mainly determined during the initial time of reaction at high initial TC concentrations. It has been determined that weak acidic conditions (pH: 3–6.5) promote the dehydration of the hydrogen at position C-5 and the hydroxyl group at position C-6 in TC and OTC (Fig. 1), as well as epimers [22,30]. Same behavior was observed for EATC although the concentration of EATC was low at all different initial concentrations. A decrease in concentration of these compounds during the reaction could be due to the sorption on nZVI surface as illustrated in Fig. 8. The desorbed amount of ETC, EATC, and ATC were in the range of 52–1,500 μg L^{-1}. ATC as transformation product of TC was determined during whole reaction mainly at above 60 mg L^{-1} initial TC concentration. On the other hand, transformation products of OTC such as EOTC, α-Apo-OTC, and β-Apo-OTC during the reaction time were negligible regardless of initial OTC concentration. Therefore, the amount of transformation products was insignificant in desorbed phase. Although EOTC was measured in the range of 5.85–7.85 μg L^{-1} within the initial time (data not shown), it was not detected through the reaction time. These results showed that OTC removal was mainly resulted from the adsorption because the concentrations of OTC transformation products were low as negligible as. Fig. 9 also represents the percentage of desorbed TCs concentrations with acid (HCl) desorption after the adsorption experiments were completed. Apparently, HCl addition could desorb about only half of the adsorbed TC from the nZVI surface while this ratio was between 21 and 43% for OTC.

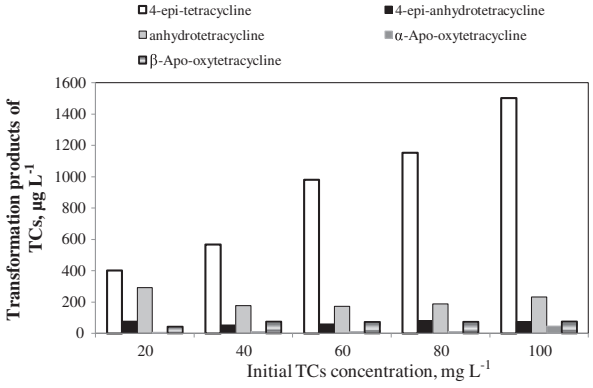

Fig. 8. The concentrations of transformation products of TC and OTC after acid desorption. ($Co_{(TC,\ OTC)}$: 20–100 mg L^{-1}, T: 30°C, pH 6, nZVI: 0.4 g L^{-1}).

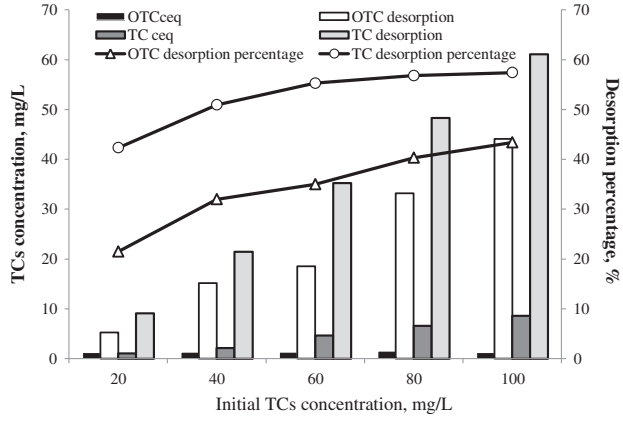

Fig. 9. TC and OTC concentrations at equilibrium time and desorbed concentration at varying initial concentrations (pH 6, equilibrium time: 2 h, nZVI: 0.4 g L^{-1}, T: 30°C).

4. Conclusion

Results from the batch studies conducted during this research demonstrate the effectiveness of nZVI for both TCs removal with different pH values, nZVI dosages, and initial concentrations. The highest removals of both TC and OTC took placed above 99% at pH 5 and 6. While TC removal was 71% at lowest dosage of 0.05 g L^{-1} nZVI, it increased to 97% at the end of 60 min with increasing nZVI dosage to 0.4 g L^{-1}. OTC removal increased from 36% at 0.05 g L^{-1} nZVI dosage to 80% at 0.4 g L^{-1} nZVI dosage. Increase in both TCs removal efficiency improved with the increase in initial nZVI dosage. The sorption rate and maximum adsorption capacity increased with an increase in the temperature for both TC and OTC. TC adsorption was higher than OTC. The dominant transformation product for TC was ETC as the transformation products for OTC were negligible. Desorption results showed that TC and OTC removal mechanism was mainly resulted from the adsorption. Kinetic results also demonstrate that the degradation of TCs by nZVI followed a pseudo- second-order model, and the adsorption data obtained by nZVI fitted reasonably well the Langmuir isotherm for both TC and OTC.

Acknowledgments

This paper includes a part of MSc thesis data of Hande Turk. The authors gracefully acknowledge the financial support from the Scientific and Technological Research Council of Turkey (TUBİTAK), Project Number 111Y092.

References

[1] C.-B. Wang, W.-X. Zhang, Synthesizing nanoscale iron particles for rapid and complete dechlorination of TCE and PCBs, Environ. Sci. Technol. 31 (1997) 2154–2156.

[2] X. Zhang, Y. Lin, Z. Chen, 2-4-6-Trinitrotoluene reduction kinetics in aqueous solution using nanoscale zero-valent iron, J. Hazard. Mater. 165 (2009) 923–927.
[3] D.W. Elliott, H.L. Lien, W.X. Zhang, Degradation of lindane by zero-valent iron nanoparticles, J. Environ. Eng. 135 (2009) 317–324.
[4] J. Fan, Y. Guo, J. Wang, M. Fan, Rapid decolorization of azo dye methyl orange in aqueous solution by nanoscale zerovalent iron particles, J. Hazard. Mater. 166 (2009) 904–910.
[5] M. Rivero-Huguet, W.D. Marshall, Reduction of hexavalent chromium mediated by micro and nano-sized mixed metallic particles, J. Hazard. Mater. 169 (2009) 1081–1087.
[6] Z. Fang, J. Chen, X. Qiu, X. Qiu, W. Cheng, L. Zhu, Effective removal of antibiotic metronidazole from water by nanoscale zero-valent iron particles, Desalination 268 (2011) 60–67.
[7] H. Chen, H. Luo, Y. Lan, T. Dong, B. Hu, Y. Wang, Removal of tetracycline from aqueous solutions using polyvinylpyrrolidone (PVP-K30) modified nanoscale zero valent iron, J. Hazard. Mater. 192 (2011) 44–53.
[8] L. Wollenberger, B. Halling-Sorenson, K.O. Kusk, Acute and chronic toxicity of veterinary antibiotics to *Daphnia magna*, Chemosphere 40 (2000) 723–730.
[9] P.K. Jiemba, The potential impact of veterinary and human therapeutic agents in manure and biosolids on plants grown on arable land: A review, Agric. Ecosyst. Environ. 93 (2002) 267–278.
[10] B. Halling Sorensen, G. Sengelov, F. Ingerslev, L.B. Jensen, Reduced antimicrobial potencies of oxytetracycline, tylosin, sulfadizine, streptomycin, ciprofloxacin and olaquindox due to environmental processes, Arch. Environ. Contam. Toxcol. 44 (2003) 7–16.
[11] M. Hammad Khan, H. Baeand J.-Y. Jung, Tetracycline degradation by ozonation in the aqueous phase: Proposed degradation intermediates and pathway, J. Hazard. Mater. 181 (2010) 659–665.
[12] D. Belkheiri, F. Fourcade, F. Geneste, D. Floner, H. At-Amar, A. Amrane, Feasibility of an electrochemical pre-treatment prior to a biological treatment for tetracycline, Sep. Purif. Technol. 83 (2011) 151–156.
[13] C.V. Gomez-Pacheco, M. Sanchez-Polo, J. Rivera-Utrilla, J.J. Lopez-Penalver, Tetracycline degradation in aqueous phase by ultraviolet radiation, Chem. Eng. J. 187 (2012) 89–95.
[14] V. Maroga-Mboula, V. Hequet, Y. Gru, R. Colin, Y. Andres, Assessment of the efficiency of photocatalysis on tetracycline biodegradation, J. Hazard. Mater. 209–210 (2012) 355–364.
[15] K.J. Choi, S.-G. Kim, S.-H. Kim, Removal of tetracycline and sulfonamide classes of antibiotic compound by powdered activated carbon, Environ. Technol. 29 (2008) 333–342.
[16] P.-H. Chang, Z. Li, T.-L. Yu, S. Munkhbayer, T.-H. Kuo, Y.-C. Hung, J.-S. Jean, K.-H. Lin, Sorptive removal of tetracycline from water by palygorskite, J. Hazard. Mater. 165 (2009) 148–155.
[17] L. Ji, W.W. Chen, J. Bi, S. Zheng, Z. Xu, D. Zhu, P. Alvarez, Adsorption of tetracycline on single-walled and multi-walled carbon nanotubes as affected by aqueous solution chemistry, Environ. Toxicol. Chem. 29(12) (2010) 2713–2719.
[18] Y. Zhao, J. Geng, X. Wang, X. Gu, S. Gao, Adsorption of tetracycline onto goethite in the presence of metal cations and humic substances, J. Colloid Interface Sci. 361 (2011) 247–251.
[19] D. Zhang, H. Niu, X. Zhang, Z. Meng, Y. Cai, Strong adsorption of chlorotetracycline on magnetite nanoparticles, J. Hazard Mater. 192 (2011) 1088–1093.
[20] Y. Gao, Y. Li, L. Zhang, H. Huang, J. Hu, S-M. Shah, X. Su, Adsorption and removal of tetracycline antibiotics from aqueous solution by graphene oxide, J. Colloid Interface Sci. 368 (2012) 540–546.
[21] Y.-H. Hwang, D.-G. Kim, H.-S. Shin, Effects of synthesis conditions on the characteristics and reactivity of nano scale zero valent iron, Appl. Catal., B, 105 (2011) 144–150.
[22] B. Halling-Sorensen, G. Sengelov, J. Tjrnelund, Toxicity of tetracyclines and tetracycline degradation products to environmentally relevant bacteria, including selected tetracycline-resistant bacteria, Arch. Environ. Contam. Toxcol. 42 (2002) 263–271.
[23] H.L. Lien, W.X. Zhang, Nanoscale iron particles for complete reduction of chlorinated ethenes, Colloids Surf. A, 191 (2001) 97–105.
[24] Y.-H. Shih, C.-Y. Hsu, Y.-F. Su, Reduction of hexachlorobenzene by nanoscale zero-valent iron: Kinetics, pH effect and degradation mechanism, Sep. Purif. Technol. 76 (2011) 268–274.
[25] Y.H. Shih, Y.C. Chen, M.Y. Chen, Y.T. Tai, C.P. Tso, Dechlorination of hexachlorobenzene by using nanoscale Fe and nanoscale Pd/Fe bimetallic particles, Colloids Surf. A, 332 (2009) 8489.
[26] W.-R. Chen, C.-H. Huang, Adsorption and transformation of tetracycline antibiotics with aluminum oxide, Chemosphere 79 (2010) 779–785.
[27] L. Zhang, X. Song, X. Liu, L. Yang, F. Pan, J. Lv, Studies on the removal of tetracycline by multi-walled carbon nanotubes, Chem. Eng. J. 178 (2011) 26–33.
[28] P.-H. Chang, J.-S. Jean, W.-T. Jiang, Z. Li, Mechanism of tetracycline sorption on rectorite, Colloids Surf. A, 339 (2009) 94–99.
[29] X.-R. Xu, X.-Y. Li, Sorption and desorption of antibiotic tetracycline on marine sediments. Chemosphere 78 (2010) 430–436.
[30] A. Jia, Y. Xiao, J. Hu, M. Asami, S. Kunikane, Simultaneous determination of tetracyclines and their degradation products in environmental waters by liquid chromatography-electrospray tandem mass spectrometry, J. Chromatogr. A 1216 (2009) 4655–4662.